Inorganic Chemistry Communications 24 (2012) 118–124

Contents lists available at SciVerse ScienceDirect

Inorganic Chemistry Communications

journal homepage: www.elsevier.com/locate/inoche

Design and synthesis of heteroleptic ruthenium (II) complexes and their applications in nanocrystalline TiO_2 solar cells

Kasim Ocakoglu [a,*], Ersan Harputlu [a], Pinar Guloglu [b], Sule Erten-Ela [b,*]

[a] Advanced Technology Research & Application Center, Mersin University, Ciftlikkoy Campus, TR-33343 Yenisehir, Mersin, Turkey
[b] Solar Energy Institute, Ege University, Bornova, 35100 Izmir, Turkey

ARTICLE INFO

Article history:
Received 10 May 2012
Accepted 11 August 2012
Available online 18 August 2012

Keywords:
Ruthenium complexes
Dye sensitized solar cells
AFM

ABSTRACT

Two ruthenium complexes, $[Ru^{II}(L2)(dcbpy)(NCS)_2]$ Ru^{II}(4,5-diazafluoren-9-one)(4,4′-dicarboxy-2,2′-bipyridyl)-di(thiocyanate) [K30] and $[Ru(dcbpy)_3]$ Ru^{II}tris(4,4′-dicarboxy-2,2′-bipyridyl) [K303] have been synthesized and used in dye sensitized solar cells. The ruthenium complexes have been characterized by elemental analyses, FT-IR, UV–Vis, cyclic voltammetry and ^{1}H NMR spectral methods. The performance of this complexes as charge transfer photosensitizer in nc-TiO_2 based dye sensitized solar cells is studied under standard AM 1.5 sunlight and by using an electrolyte consisting of 0.6 M *N*-methyl-*N*-butyl imidazolium iodide (BMII), 0.1 M LiI, 0.05 M I_2, 0.5 M 4-*tert*-butyl pyridine (TBP) in acetonitrile. Notably, the photo-to-electrical conversion efficiency of the DSSCs sensitized with [K30] and [K303] reaches 3.45%, and 6.33%, and the DSSC sensitized with [K303] shows better photovoltaic performances (Jsc = 19.58 mA/cm^2, Voc = 570 mV and FF = 0.58) than [K30].

The rapidly increasing fossil fuel consumption and excessive greenhouse gas emissions have put significant pressure on the already exhaustive global energy demand and needs for environmental protection. The global growing demand for energy and for protecting our environment can potentially be met by solar cell technology. Solar cells are promising devices in search of sustainable renewable sources of energy. Although silicon cells based on solid-state p–n junction devices have dominated the field, a new generation of photovoltaics is emerging. Since the original model cell reported by O'Regan and Graetzel in 1991, almost 21 years of research in the field of photoelectrochemical cells have led to the development of efficient and low-cost dye sensitized solar cells (DSSCs) at the laboratory level. Although the solar cells technology has not yet been in large-scale utilization because of its high cost and insufficient conversion efficiencies in the past, recent advances in nanomaterial and device technologies have offered new opportunities for it to become competitive to fossil fuels. Among the diverse photovoltaic devices, the dye sensitized solar cells (DSSCs) technology has made enormous progresses and is highly competitive for large-scale commercial fabrication. DSSCs have emerged as an attractive choice for solar energy harvesting since their invention [1,2]. Dye sensitized solar cells (DSSCs) created from nanocrystalline TiO_2 films have been intensively investigated over the past decade. The critical component in DSSCs is the photoanode, which is typically composed of a porous TiO_2 or ZnO nanoparticle film with dye molecules adsorbed onto its surface. To achieve high performance, the photoanode needs to possess a large surface area and good electron transport capability. A TiO_2 or ZnO nanoparticle film provides a large enough surface area; however, electron transport is difficult because of the need for electrons to hop across neighboring nanoparticles. Moreover, it is well-known that semiconducting particle surfaces are prone to form defects that can act as electron trapping centers. The presence of these surface traps is detrimental to electron transport because trapping/detrapping events are unavoidable during electron diffusion through the disordered nanoparticle network. By altering the morphology of the photoanode, electron transport pathways may be designed to improve electron collection [3,4]. Since the sensitizers used in DSSCs are critical to the cell's photovoltaic performance, extensive efforts have been focused on the synthesis of new, highly efficient sensitizers. Among the numerous sensitizers developed for this purpose, ruthenium(II) polypyridine complexes have received much attention owing to their superior performance in DSSCs. Ruthenium(II) polypyridyl complexes have been widely investigated for their use as sensitizers in DSSCs, since Grätzel and coworkers reported their remarkable properties. Among the sensitizer as one of the key components for high power conversion efficiency, the most efficient and successful sensitizers are ruthenium(II) complexes. They also have suitable ground- and excited-state energy levels with respect to the nanocrystalline TiO_2 conduction-band energy and they match the redox properties of the iodine/triiodide redox couple [5–7].

* Corresponding authors.
E-mail addresses: kasimocakoglu@gmail.com, kasim.ocakoglu@mersin.edu.tr (K. Ocakoglu), suleerten@yahoo.com, sule.erten@ege.edu.tr (S. Erten-Ela).

1387-7003/$ – see front matter © 2012 Elsevier B.V. All rights reserved.
http://dx.doi.org/10.1016/j.inoche.2012.08.006

We report here the synthesis and characterization of ruthenium sensitizers in an attempt to gain more comprehensive insight into the chemical and physical nature of the molecular functionality on solar energy conversion efficiency. Schematic illustration of DSSCs is presented in Fig. 1.

The structures of the ruthenium complexes are identified by infrared spectroscopy (FTIR), elemental analysis, nuclear magnetic resonance (NMR) spectroscopy. All commercially available chemicals and solvents are used without further purification. Synthetic details and NMR data of ligands ruthenium complexes are described here. Synthesis of Ru^{II} tris(4,4′-dicarboxy-2,2′-bipyridyl), [Ru(dcbpy)$_3$], [K303]; [$RuCl_2$(*p*-cymene)]$_2$ (0.1 g, 0.16 mmol) was dissolved in DMF (50 mL) under inert atmosphere, and dcbpy (0.117 g, 0.48 mmol) then added. The reaction mixture was heated to 60 °C under argon for 4 h with constant stirring, and then refluxed for 3 days. The reaction mixture was cooled down to room temperature and the solvent was removed by using a rotary evaporator under vacuum. The solid was extracted with methanol, filtered and dried under vacuum. Purification on Sephadex LH20 afforded the desired complex as a dark purple solid. 168 mg, 63% yield. Anal. Calc. For $RuC_{36}H_{24}Cl_2N_6O_{12}$: C, 47.80; H, 2.67; N, 9.29. Found: C, 47.78; H, 2.65; N, 9.28%. FT-IR (KBr, cm^{-1}): 1671, 1613, 1554, 1513, 1420, 1391, 1261, 1100, 1054, 938, 862, 846, 780, 729, 680, 635, 556, 476. ^{1}H NMR (DMSO) δ ppm: 9.53 (d, J = 5.9 Hz, 6H, CC*H*CHN); 8.89 (s, 3H, CC*H*C); 8.74. (s, 3H, CC*H*C); 7.74 (d, J = 6 Hz, 6H, CCHC*H*N). K303 was synthesized according to a modified literature method [8]. However, in our study we used [$RuCl_2$(*p*-cymene)]$_2$ as a precursor, and a chloride salt of the complex, [Ru(dcbpy)$_3$]Cl_2, was obtained at the end of the synthesis unlike that mentioned in the previous method [8]. Dabestani et al. reported the synthesis of PF_6 salt of the complex, [Ru(dcbpy)$_3$]PF_6 for light emitting diode applications. On the other hand, in general chloride salt is preferred in dye sensitized solar cell application. Synthesis of Ru^{II}(4,5-diazafluoren-9-one)(4,4′-dicarboxy-2,2′-bipyridyl)-di(thiocyanate), [Ru^{II}(L2)(dcbpy)$(NCS)_2$], [K30]; [$RuCl_2$(*p*-cymene)]$_2$ (0.1 g, 0.16 mmol) was dissolved in DMF (50 mL) under inert atmosphere, and 4,5-diazafluoren-9-one (L3) (0.0585 g, 0.32 mmol) then added. The reaction mixture was heated to 60 °C for 4 h with constant stirring. The reaction mixture was heated to 60 °C under argon for 4 h with constant stirring. To this reaction flask dcbpy (0.08 g, 0.32 mmol) was added and refluxed for 4 h. Finally, excess of NH_4SCN (0.988 g, 13 mmol) was added to the reaction mixture and the reflux continued for another 4 h. The reaction mixture was cooled down to room temperature and the solvent was removed by using a rotary evaporator under vacuum. Water was added to the flask and the insoluble solid was collected on a sintered glass crucible by suction filtration. The solid was dried under vacuum. The crude complex was re-crystallized from methanol and diethyl ether. 183 mg, 89 % yield.

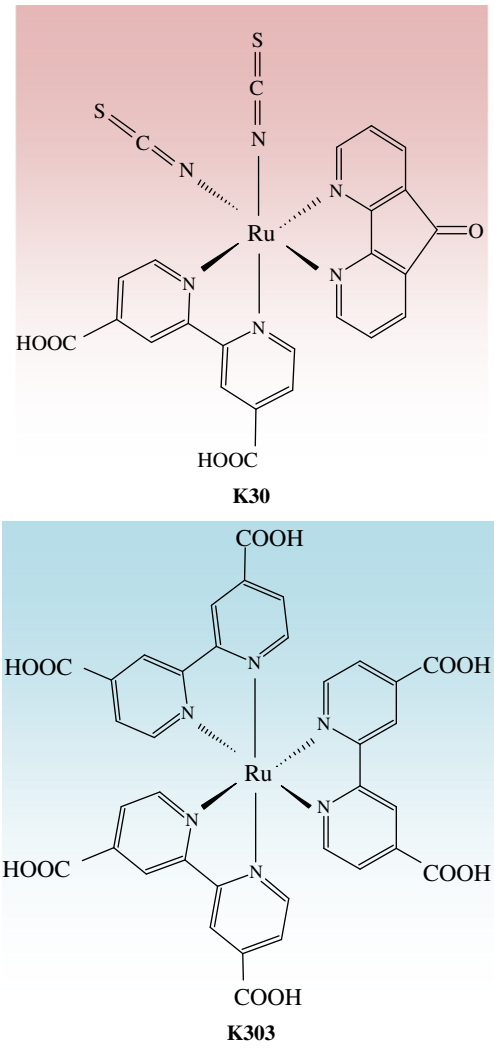

Fig. 2. Chemical structures of the ruthenium complexes.

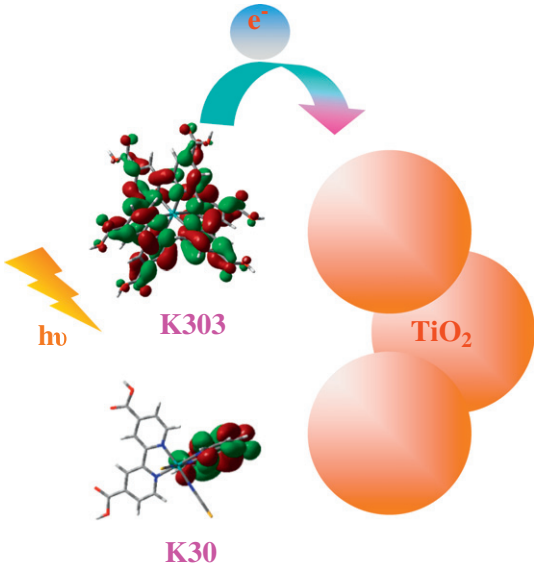

Fig. 1. Schematic illustration of DSSC.

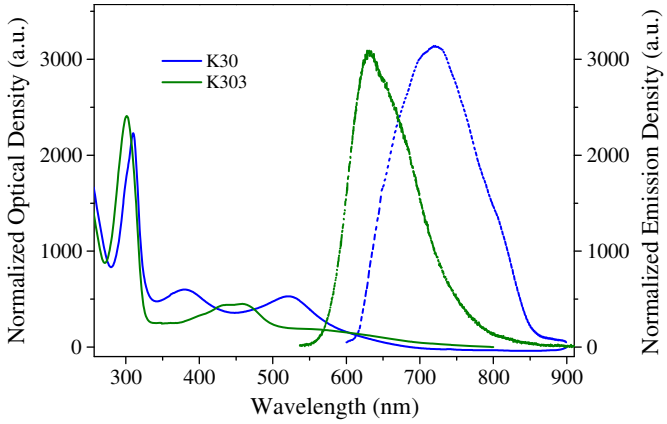

Fig. 3. UV–Vis absorption (solid lines) and steady-state fluorescence spectra (dashed lines) of K30 and K303 measured in DMF, λ_{ex}: 400 nm for K30, λ_{ex}: 470 nm for K303.

Table 1
UV–Vis apsorption and emission properties of ruthenium complexes. K30 and K303 measured in DMF.

	λ_{max}, (nm) ($\varepsilon/10^4$ $M^{-1}.cm^{-1}$)		Emisyon λ_{max}, (nm)
	L (π–π^*)	4d–π^*	
K30	306 (3.26)	380 (1.07), 524 (1.03)	720
K303	301 (5.65)	433 (1.03), 458 (1.06), 563 (0.43)	630

Anal. Calc. For $RuC_{25}H_{14}Cl_2N_6O_5S_2$: C, 42.02; H, 1.97; N, 11.76. Found: C, 42.04; H, 1.94; N, 11.74. FT-IR (KBr, cm^{-1}): 3414, 3109, 2789, 2112, 2061, 1711, 1595, 1401, 1371, 786. ^{1}H NMR (DMSO) δ ppm: 9.50 (d, J=6 Hz, 1H, NC*H*CH), 9.27 (d, J=5.2 Hz, 1H, NC*H*CH), 8.44 (s, 1H, CC*H*C), 8.25 (s, 1H, CC*H*C), 8.01 (d, J=7.4 Hz, 1H, CHC*H*C), 7.84 (d, J=7.4 Hz, 1H, CHC*H*C), 7.65 (d, J=5.2 Hz, 1H, NC*H*CH), 7.61 (d, J=6 Hz, 1H, CC*H*CH), 7.58 (d, J=4 Hz, 1H, NC*H*CH), 7.13 (q, J=5.2 Hz, 1H, CHC*H*CH), 7.02 (d, J=1.6 Hz, 1H, CC*H*CH), 6.49 (q, J=5.2 Hz, 1H, CHC*H*CH). Fig. 2 shows the chemical structure of ruthenium complexes for K30 and K303.

Fig. 3 shows the absorption and emission spectra of the complexes measured in *N*, *N*-dimethylformamide (DMF) solution. Table 1 summarizes absorption and emission properties of two ruthenium complexes. All complexes show broad and intense absorption bands between 380 and 563 nm, due to metal to ligand charge transfer transitions (MLCT) (Table 1) [9]. In the UV region the complexes show distinct intra ligand (π–π^*) charge transfer transitions at 306 and 301 nm for K30 and K303, respectively, that are assigned to L2 and dcbpy ligands [10]. When the complexes are excited within the MLCT absorption band at 298 K in an air-equilibrated DMF solution (for K303, in 0.1 M NaOH/DMF), they exhibit luminescence maxima at 720 (K30) and 630 nm (K303), respectively.

The cyclic voltammograms are collected using a CH-Instrument 660 B Model electrochemical analyzer. The electrochemical properties of the ruthenium complexes are examined by cyclic voltammetry in DMF solvent with 0.1 M $TBAPF_6$ using a glassy carbon electrode. All redox potentials are calibrated *vs.* SCE. The results are collected in Table 2, and cyclic voltammograms are shown in Fig. 4. The cyclic voltammograms of the complexes, K30 and K303, show reversible waves at 1.08 and 1.37 *vs.* SCE, which are attributed to the Ru(III/II) redox couple [11,12]. The Ru(III/II) redox potential of K303 complex is more positive than that of K30 complex. The reason for this positive shift is due to π-acceptor nature of dcbpy ligands. The reduction peaks of the complexes are observed −0.73 V, −1.18 V for K30 and K303, respectively. These values correspond to reductions of carbonyl groups. The difference between the reduction potentials is related to the number of carbonyl groups, and different electron donor and acceptor behaviors of the ligands [13,14].

Ground state optimization of complexes is shown in Fig. 5 and experimental and calculated E_{HOMO} and E_{LUMO} energy levels of ruthenium complexes are shown in Fig. 6.

All ground-state geometry optimization calculations are performed with the Gaussian 03 program (Fig. 6) package employing the DFT

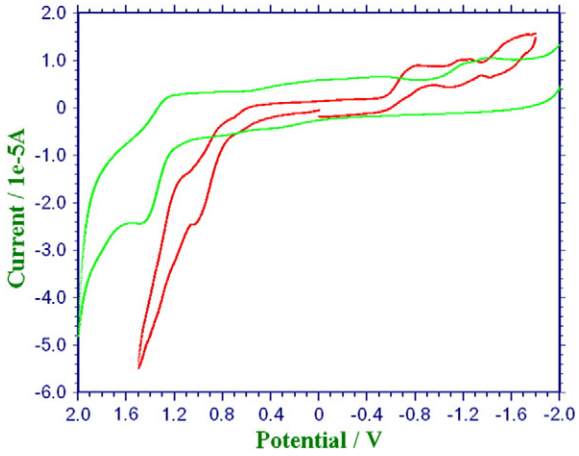

Fig. 4. Cyclic voltammogram of ruthenium complexes.

method with Becke's three parameter hybrid functional [15] and Lee–Yang–Parr's gradient corrected correlation functional (B3LYP) [16]. The LanL2DZ basis set [17] and effective core potential used for the Ru atom basis set [18] are applied for all other atoms. In addition, in order to obtain the vertical excitation energies of the complexes, single point time dependent density functional theory (TD-DFT) [19] using B3LYP is utilized with LANL2DZ basis set by using its ground state DFT geometries.

Tables 3 and 4 give the vertical excitation energies, corresponding excitation wavelengths and oscillator strengths, predominant orbitals involved in ten singlet–singlet transitions and their characters obtained from the single point TD-DFT calculations for K30 and K303. The molecular orbital (MO) plots of the K303 and K30 molecules involved in the lowest 10 energy CT transitions ($S_0 \rightarrow S_1$, $S_0 \rightarrow S_2$, $S_0 \rightarrow S_3$, $S_0 \rightarrow S_4$, $S_0 \rightarrow S_5$, $S_0 \rightarrow S_6$, $S_0 \rightarrow S_7$, $S_0 \rightarrow S_8$, $S_0 \rightarrow S_9$ and $S_0 \rightarrow S_{10}$) are displayed in Figs. 6, 7, Tables 4 and 5.

As clearly seen from Fig. 6, HOMO − 3, HOMO − 2, HOMO − 1 and HOMO are completely localized on the donor RuNCS group and LUMO+3, LUMO+2, LUMO+1 and LUMO are localized on the acceptor –COOH group and it is clear that the HOMO–LUMO transitions of K303 will have $\pi \rightarrow \pi^*$ character.

The surface morphology of ruthenium complexes on mica is examined by atomic force microscopy (AFM) in non-contact mode under ambient conditions (Fig. 8), and the obtained AFM topographic images are analyzed by the XEI program. The samples are prepared in DMF (for K303, 0.1 M NaOH/DMF) with a concentration of 1.5×10^{-5} M. A freshly prepared solution is deposited by drop-casting on a mica surface, and then letting the drop dry at room temperature in ambient air conditions. AFM studies on mica surfaces exhibited the relatively ordered spherical morphology (Fig. 8). The individual bright objects that exhibit a spherical morphology can be attributed to the strong hydrogen bond formation ability of the functional groups of the

Table 2
Redox potentials and E_{HOMO} and E_{LUMO} levels of ruthenium complexes.

	$E_{oxidation}$ [a] (Volt)	$E_{reduction}$ [b] (Volt)	$E_{ferrocene}$ [c] (Volt)	E_{HOMO} [d] (eV)	E_{LUMO} [e] (eV)	$E_{Band\ Gap}$ [f]
K30	1.08	−0.73	0.44	5.44	3.63	1.81
K303	1.37	−1.18	0.45	5.72	3.17	2.55

[a] First oxidation potentials of Ru complexes.
[b] Reduction potentials of Ru complexes.
[c] Potentials of ferrocene, internal reference electrode.
[d] HOMO energy level of Ru complexes.
[e] LUMO energy level of Ru complexes.
[f] Energy band gap of Ru complexes.

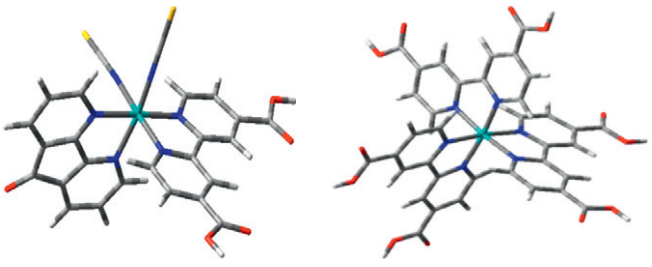

Fig. 5. Ground state optimization at B3LYP/LANL2DZ.

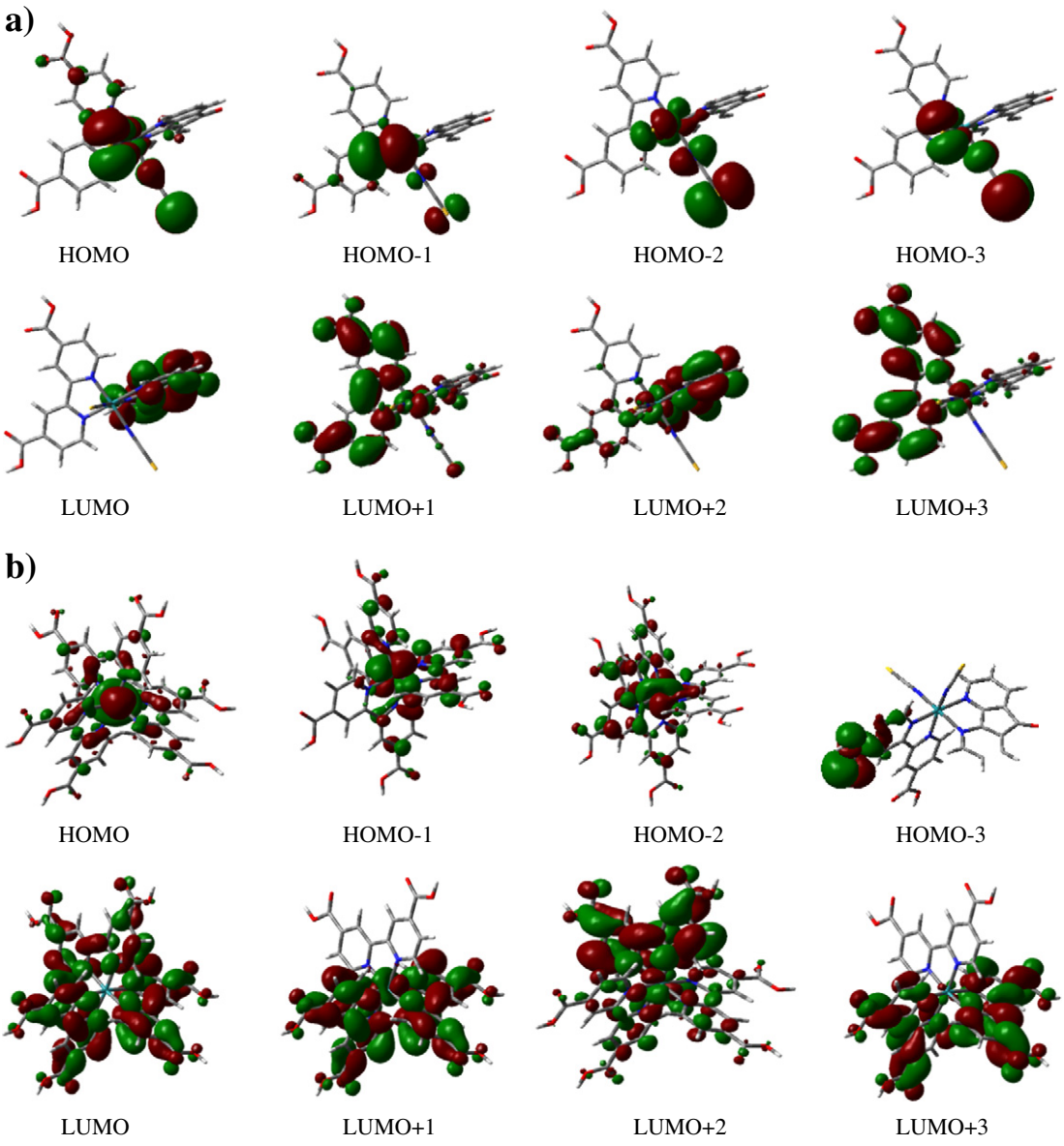

Fig. 6. Schematic representation of the molecular orbitals of [K30] (a) and [K303] (b) obtained from DFT (B3LYP/LANL2DZ) method.

ligands, such as –COOH. Moreover, layered salt form of the compound K303 can be easily distinguished from AFM image due to sodium acetate formation (0.1 M NaOH/DMF).

A nanocrystalline TiO_2 photoelectrode is prepared by screen printing on conductive glass. Preparation and characterization of double-layer TiO_2 electrode are previously described by Wang [20] et al. FTO (SnO_2:F, Pilkington TEC-15; Rsheet:15O/&), electrically conductive oxide-coated glasses are used as transparent electrodes. The construction of the dye sensitized solar cell device requires first cleaning of the fluorine doped tin oxide (FTO) coated glass substrates in a detergent solution using an ultrasonic bath for 15 min, rinsed with water and ethanol. Both sensitizers have been used to manufacture solar cell devices to explore current–voltage characteristics using 7(transparent) + 5(scattering) μm TiO_2 transparent layers. TiO_2-coated electrodes, after sintering at 450 °C for 30 min and cooling to 100 °C, are immersed into the solution of 0.5 mM ruthenium complexes in a mixture of DMF:acetonitrile:tert-butanol (volume ratio: 3:1:1) and kept at room temperature overnight. Ruthenium complexes adsorbed TiO_2-coated glasses are washed with pure chlorobenzene. The stained electrode and Pt-counter electrode are assembled into a sealed sandwich-type cell by heating with a hot-melt ionomer film (Surlyn 1702, DuPont) as a spacer between the electrodes. Platinized FTO glasses are used as counter electrode. Platinization of counter electrodes is done by coating of FTO glasses with 1% solution of hydrogen hexachloroplatinate (Aldrich) in 2-propanol and annealing at 400 °C for 30 min. Cells are prepared in sandwich geometry. Surlyn-1702 (DuPont) frame is used as a spacer and a thermoplastic sealant between the two electrodes. Cells prepared in this way are then sealed by heating at 100 °C. A drop of electrolyte solution (electrolyte of 0.6 M *N*-methyl-*N*-butyl-imidazolium iodide (BMII) + 0.1 M LiI + 0.05 M I_2 + 0.5 M 4-*tert*-butylpyridine (TBP) in acetonitrile) is placed on the drilled hole in the counter electrode of the assembled cell and is driven into the cell via vacuum backfilling. Finally, the hole is sealed using additional Bynel and a cover glass (0.1 mm thickness). Active areas of the cells are adjusted to 0.159 cm^2. Photovoltaic experiments are performed under AM 1.5 irradiation (100mWcm^{-2}). J−V data collection is made by using Keithley 2400 Source-Meter and LabView data acquisition software. J−V

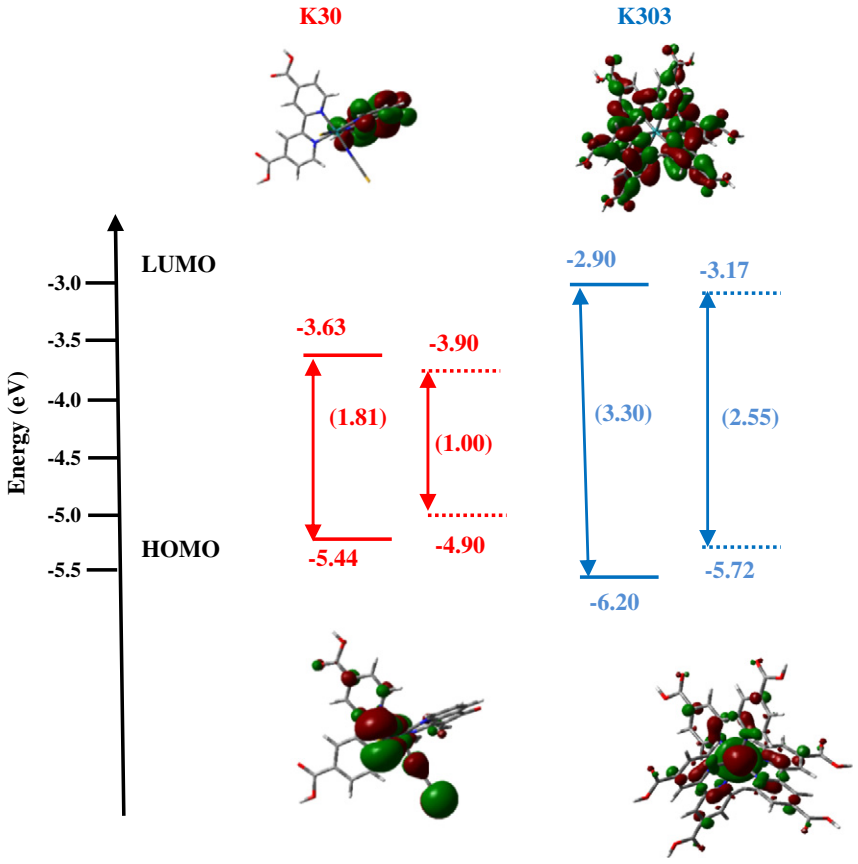

Fig. 7. Schematic representation of frontier orbitals of K30 and K303, along with isodensity plots of HOMO and LUMO orbitals. The experimental and calculated energy levels are displayed in solid and dashed line, respectively.

characteristics of dye sensitized solar cell in dark and under illumination is shown in Fig. 9. And photovoltaic characterizations of ruthenium complexes are summarized in Table 5. The results for DSSCs of K30 and K303 are as follows: short-circuit photocurrent = 9.77 and 19.58 mA cm^{-2}; open-circuit voltages = 530 mV and 570 mV; fill factor = 0.64 and 0.58; and overall solar-light-to-electrical-conversion efficiency =

Table 3
Calculated properties of electronically excited states of [K30].

State	ΔE (eV)	λ_{exc} (nm)	Oscillator strength (f)	Predominant transitions	Character
$S_0 \rightarrow S_1$	0.4810	2577.66	0.0013	(HOMO) → (LUMO)	CT[a] (COOH–CO)
$S_0 \rightarrow S_2$	0.6362	1948.69	0.0013	(HOMO − 1) → (LUMO)	CT (RuNCS–CO)
$S_0 \rightarrow S_3$	0.6810	1820.54	0.0004	(HOMO − 2) → (LUMO)	CT (RuNCS–CO)
$S_0 \rightarrow S_4$	0.7863	1576.76	0.0003	(HOMO − 3) → (LUMO)	CT (RuNCS–CO)
$S_0 \rightarrow S_5$	0.9264	1338.27	0.0103	(HOMO) → (LUMO+1)	CT (RuNCS–COOH)
$S_0 \rightarrow S_6$	1.1406	1086.95	0.0019	(HOMO − 2) → (LUMO+1)	CT (RuNCS–COOH)
$S_0 \rightarrow S_7$	1.1567	1071.87	0.0179	(HOMO) → (LUMO+2)	CT (RuNCS–CO)
$S_0 \rightarrow S_8$	1.2177	1018.17	0.0162	(HOMO − 1) → (LUMO+1)	CT (RuNCS–COOH)
$S_0 \rightarrow S_9$	1.3284	933.31	0.0126	(HOMO − 3) → (LUMO+1)	CT (RuNCS–COOH)
$S_0 \rightarrow S_{10}$	1.3522	916.89	0.0094	(HOMO − 1) → (LUMO+1)	CT (RuNCS–CO)

[a] CT: charge transfer.

Table 4
Calculated properties of electronically excited states of [K303].

State	ΔE (eV)	λ_{exc} (nm)	Oscillator strength (f)	Predominant transitions	Character
$S_0 \rightarrow S_1$	2.4197	512.39	0.0048	(HOMO) → (LUMO)	CT[a] (Ru–COOH)
$S_0 \rightarrow S_2$	2.4236	511.56	0.0014	(HOMO) → (LUMO+1)	CT (Ru–COOH)
$S_0 \rightarrow S_3$	2.4625	503.48	0.0025	(HOMO) → (LUMO+1)	CT (Ru–COOH)
$S_0 \rightarrow S_4$	2.5959	477.62	0.0024	(HOMO − 2) → (LUMO)	CT (Ru–COOH)
$S_0 \rightarrow S_5$	2.6248	472.36	0.0081	(HOMO − 1) → (LUMO)	CT (Ru–COOH)
$S_0 \rightarrow S_6$	2.6567	466.68	0.0157	(HOMO − 2) → (LUMO)	CT (Ru–COOH)
$S_0 \rightarrow S_7$	2.7871	444.86	0.1554	(HOMO − 2) → (LUMO+2)	CT (Ru–COOH)
$S_0 \rightarrow S_8$	2.8057	441.90	0.1656	(HOMO − 2) → (LUMO+1)	CT (Ru–COOH)
$S_0 \rightarrow S_9$	3.0058	412.49	0.0008	(HOMO − 1) → (LUMO+2)	CT (Ru–COOH)
$S_0 \rightarrow S_{10}$	3.3394	371.27	0.0624	(HOMO) → (LUMO+3)	CT (Ru–COOH)

[a] CT: charge transfer.

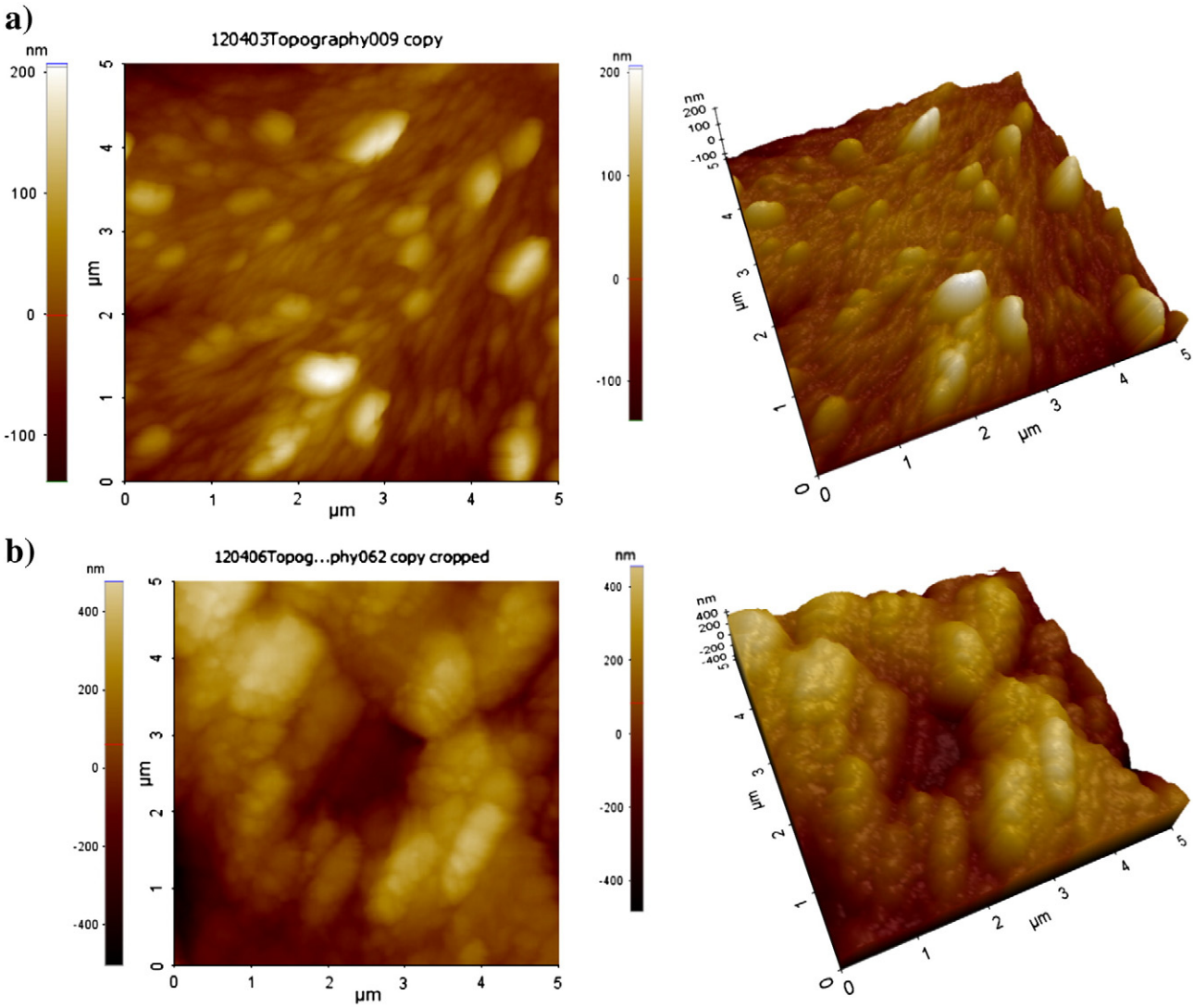

Fig. 8. AFM topographic images in non-contact mode of Ru–PC film. Samples are prepared by drop-casting of the solutions of the complex ($c = 1.5 \times 10^{-5}$ M) in DMF onto mica substrate and measured in air. K303 (a), K30 (b).

3.45% and 6.33%, respectively. The higher Voc of K303 is probably to be traced back to its adsorption geometry, which can exploit binding via three carboxylic groups. This is in analogy to a related complex where phosphonic acid anchoring groups are employed in place of carboxylic groups [21–23].

In summary, in this paper we report the complexes of ruthenium dye as well as their DSSC characterization. K303 ruthenium complex is found as more efficient sentitizer in DSSCs compared to K30 ruthenium complex. The higher efficiency of DSSC sensitized with the K303 dye can be attributed to higher electron injection yield and slower charge recombination rate due to carboxylic groups avoiding the aggregation on TiO_2 surface. The selections of carboxylic acid groups in K303 complex are supplied to suppress charge recombination compared to the selection of 4,5-diazafluoren-9-one group and carboxyl group of K30 ruthenium complex. Furthermore, K303 ruthenium complex based dye sensitized solar cell using TiO_2 electrode yielded corresponding to a higher overall conversion efficiency (η) of 6.33%.

Table 5
Photovoltaic performances of the compounds under 100 mW/cm^2 light intensity and AM1.5 global radiation.

Sample	I_{sc} (mA/cm^2)	V_{oc} (mV)	η (%)	FF
K30	9.77	530	3.45	0.64
K303	19.58	570	6.33	0.58

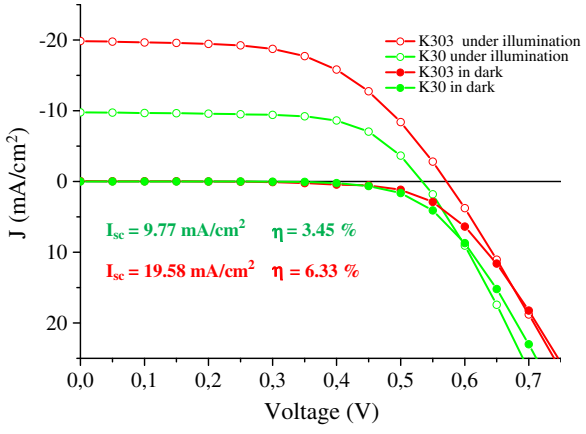

Fig. 9. J–V curve of TiO_2 based dye sensitized solar cells.

References

[1] B. O'Regan, M. Gratzel, A low-cost, high-efficiency solar cell based on dye-sensitized colloidal TiO_2 films, Nature 353 (1991) 737–740.

[2] A.C. Fisher, L.M. Peter, E.A. Ponomarev, A.B. Walker, K.G.U. Wijayantha, Intensity dependence of the back reaction and transport of electrons in dye-sensitized nanacrystalline TiO_2 solar cells, J. Phys. Chem. B. 104 (2000) 949–958.

[3] G.M. Turner, M.C. Beard, C.A. Schmuttenmaer, Carrier localization and cooling in dye-sensitized nanocrystalline titanium dioxide, J. Phys. Chem. B. 106 (2002) 11716–11719.

[4] J. Lagemaat, A.J. Frank, Nonthermalized electron transport in dye-sensitized nanocrystalline TiO_2 films: transient photocurrent and random-walk modeling studies, J. Phys. Chem. B. 105 (2001) 11194–11205.

[5] S. Wenger, P.A. Bouit, Q. Chen, J. Teuscher, D.D. Censo, R. Humphry-Baker, J.E. Moser, J.L. Delgado, N. Martin, S.M. Zakeeruddin, M. Graetzel, Efficient electron transfer and sensitizer regeneration in stable π-extended tetrathiafulvalene-sensitized solar cells, J. Am. Chem. Soc. 132 (2010) 5164–5169.

[6] K. Hara, K. Sayama, H. Arakawa, Y. Ogha, A. Shinpo, S. Suga, A coumarin-derivative dye sensitized nanocrystalline TiO_2 solar cell having a high solar-energy conversion efficiency up to 5.6%, Chem. Commun. 37 (2001) 569–570.

[7] P.-A. Bouit, D. Rauh, S. Neugebauer, J. Luis Delgado, E. Di Piazza, S. Rigaut, O. Maury, C. Andraud, V. Dyakonov, N. Martin, A "cyanine−cyanine" salt exhibiting photovoltaic properties, Org. Lett. 11 (2009) 4806–4809.

[8] R. Dabestani, A.J. Bard, A. Campion, M.A. Fox, T.E. Mallouk, S.E. Webber, J.M. White, Sensitization of titanium dioxide and strontium titanate electrodes by ruthenium(I I) Tris (2,2′- bipyridine-4,4′-dicar boxylic acid) and zinc tetra kis (4-carboxy p hen yl) porphyrin: an evaluation of sensitization efficiency for component photoelectrodes in a multipanel device, J. Phys. Chem. 92 (1988) 1872–1878.

[9] V. Balzani, A. Juris, M. Venturi, S. Campagna, S. Serroni, Luminescent and redox-active polynuclear transition metal complexes, Chem. Rev. 96 (1996) 759–833.

[10] T.J. Meyer, Photochemistry of metal coordination complexes: metal to ligand charge transfer excited states, Pure Appl. Chem. 58 (1986) 1193–1206.

[11] N.P. Ayala, C.M. Flynn, L.J. Sacksteder, J.N. Demas, B.A. DeGraff, Synthesis, luminescence, and excited-state complexes of the tris(1,10-phenanthroline) iridium(III) and bis(terpyridine)iridium(III) cations, J. Am. Chem. Soc. 112 (1990) 3837–3844.

[12] G.J. Samuels, T.J. Meyer, An electrode-supported oxidation catalyst based on ruthenium(IV)-Ph encapsulation in a polymer film, J. Am. Chem. Soc. 103 (1981) 307–309.

[13] K. Ocakoglu, C. Zafer, B. Cetinkaya, S. Icli, Synthesis, characterization, electrochemical and spectroscopic studies of two new heteroleptic Ru(II) polypyridyl complexes, Dye. Pigment. 75 (2007) 385–394.

[14] (a) S. Erten-Ela, D. Yilmaz, B. Icli, Y. Dede, S. Icli, E.U. Akkaya, A panchromatic boradiazaindacene (BODIPY) sensitizer for dye-sensitized solar cells, Org. Lett. 10 (2008) 3299–3302;
(b) S. Kolemen, A. Bozdemir, Y. Cakmak, G. Barin, S. Erten-Ela, M. Marszalek, J.-H. Yum, S.M. Zakeeruddin, M.K. Nazeeruddin, M. Graetzel, E.U. Akkaya, Optimization of distyryl-bodipy chromophores for efficient panchromatic sensitization in dye sensitized solar cells, Chem. Sci. 2 (2011) 949–954;
(c) S. Kolemen, Y. Cakmak, S. Erten-Ela, Y. Altay, J. Brendel, M. Thelakkat, E.U. Akkaya, Solid-state dye-sensitized solar cells using red and near-IR absorbing bodipy sensitizers, Org. Lett. 12 (2010) 3812–3815;
(d) S. Erten-Ela, J. Brendel, M. Thelakkat, " Solid-state dye-sensitized solar cells fabricated with nanoporous TiO2 and TPD dyes: Analysis of penetration behavior and I–V characteristics, Chem. Phys. Lett. 510 (2011) 93–98.

[15] A.D. Becke, Density-functional thermochemistry. III. The role of exact exchange, J. Chem. Phys. 98 (1993) 5648–5652.

[16] C. Lee, W. Yang, R.G. Parr, Development of the Colle-Salvetti correlation-energy formula into a functional of the electron density, Phys. Rev. B. 37 (1988) 785–789.

[17] P.J. Hay, R.W. Willard, Ab initio effective core potentials for molecular calculations. Potentials for the transition metal atoms Sc to Hg, J. Chem. Phys. 82 (1985) 270–283.

[18] R. Krishnan, J.S. Binkley, R. Seeger, J.A. Pople, Self-consistent molecular orbital methods. XX. A basis set for correlated wave functions, J. Chem. Phys. 72 (1980) 650–654.

[19] E. Runge, E.K.U. Gross, Density-functional theory for time-dependent systems, Phys. Rev. Lett. 52 (1984) 997–1000.

[20] C. Li, W. Wang, X. Wang, B. Zhang, Y. Cao, Molecular design of squaraine dyes for efficient far-red and near-IR sensitization of solar cells, Chem. Lett. 34 (2005) 554–555.

[21] K. Hanson, M.K. Brennaman, A. Ito, H. Luo, W. Song, K.A. Parker, R. Ghosh, M.R. Norris, C.R.K. Glasson, J.J. Concepcion, R. Lopez, T.J. Meyer, Structure−property relationships in phosphonate-derivatized, RuII polypyridyl dyes on metal oxide surfaces in an aqueous environment, J. Phys. Chem. C 116 (2012) 14837–14847.

[22] F. De Angelis, S. Fantacci, A. Selloni, M.K. Nazeeruddin, M. Graetzel, First-principles modeling of the adsorption geometry and electronic structure of Ru(II) dyes on extended TiO_2 substrates for dye-sensitized solar cell applications, J. Phys. Chem. C 114 (2010) 6054–6061.

[23] F. De Angelis, S. Fantacci, A. Selloni, M. Graetzel, M.K. Nazeeruddin, Influence of the sensitizer adsorption mode on the open-circuit potential of dye-sensitized solar cells, Nano Lett. 10 (2007) 3189–3195.